ADVANCES IN ATMOSPHERIC SCIENCES, VOL. 40, SEPTEMBER 2023, 1558–1566

• News & Views •

Super Typhoon Hinnamnor (2022) with a Record-Breaking Lifespan over the Western North Pacific

Qian WANG[1,2,3], Dajun ZHAO[*2,5], Yihong DUAN[2], Shoude GUAN[4], Lin DONG[3], Hongxiong XU[2], and Hui WANG[2]

[1]*Department of Atmospheric and Oceanic Sciences and Institute of Atmospheric Sciences*, *Fudan University*, *Shanghai* 200433, *China*

[2]*State Key Laboratory of Severe Weather*, *Chinese Academy of Meteorological Sciences*, *Beijing* 100081, *China*

[3]*National Meteorological Centre*, *Beijing* 100081, *China*

[4]*Frontier Science Center for Deep Ocean Multispheres and Earth System (FDOMES) and Physical Oceanography Laboratory/Sanya Oceanographic Institution*, *Ocean University of China*, *Qingdao* 266100, *China*

[5]*Shanghai Typhoon Institute*, *China Meteorological Administration*, *Shanghai* 200030, *China*

(Received 6 November 2022; revised 27 January 2023; accepted 1 February 2023)

ABSTRACT

Super Typhoon Hinnamnor (2022) was a rare and unique western North Pacific typhoon, and throughout its lifespan, it exhibited all of the major features that pose current challenges in typhoon research. Specifically, during different stages of its lifespan, it experienced a sudden change of track, underwent rapid intensification, interacted and merged with another vortex, expanded in size, underwent rapid weakening, produced a strong cold wake, exhibited eyewall replacement, and underwent extratropical transition. Therefore, a timely identification and review of these features of Hinnamnor (2022), as reported in this article, will help update and enrich the case sets for each of these scientific issues and provide a background for more in-depth mechanistic studies of typhoon track, intensity, and structural changes in the future. We also believe that Hinnamnor (2022) can serve as an excellent benchmark to quickly evaluate the overall performance of different numerical models in predicting typhoon's track, intensity, and structural changes.

Key words: sudden track change, rapid intensification, rapid weakening, vortex merging, extratropical transition

Citation: Wang, Q., D. J. Zhao, Y. H. Duan, S. D. Guan, L. Dong, H. X. Xu, and H. Wang, 2023: Super Typhoon Hinnamnor (2022) with a record-breaking lifespan over the western North Pacific. *Adv. Atmos. Sci.*, **40**(9), 1558–1566, https://doi.org/10.1007/s00376-023-2336-y.

1. Introduction

The western North Pacific is the most favorable region worldwide for the genesis of tropical cyclones (TCs) with more than one-third of TCs being born there each year (Gray, 1968; Chen and Ding, 1979). Although extraordinary progress has been made in TC research and forecasting (Wang and Wu, 2004; Emanuel, 2018; Lei, 2020; Tan et al., 2022), there are still many challenges. Among these challenges, sudden changes in TC track, rapid intensification (RI) and rapid weakening (RW), and quantitative precipitation forecasting associated with landfalling TCs are the top three (Chen et al., 2010; Duan et al., 2014, 2019; Zhao et al., 2022a, b). Although track and intensity forecasts of TCs have been improved over recent decades, the operational numerical modeling and subjective forecasting of abrupt changes in track and intensity (Elsberry et al., 2013; Roger et al., 2013; DeMaria et al., 2014), especially under both RI and RW (Fei et al., 2020; Wang et al., 2022), remain challenging. Many famous recorded TC cases are remembered for their unusual tracks, their rapidly changing intensities, the extreme precipitation they brought, or the unique structural features they possessed (Chen and Ding, 1979; Chen at al., 2012; Wang, 2018). Remarkably, the lifespan of Super Typhoon Hinnamnor (2022) was characterized by all these qualities.

* Corresponding author: Dajun ZHAO
Email: zhaodajun@cma.gov.cn

Super Typhoon Hinnamnor (2022) formed in the western North Pacific Ocean near Minamitorishima Island at 0600 UTC 28 August 2022 and reached typhoon status (General Administration of Quality Supervision, Inspection and Quarantine of the People's Republic of China and Standardization Administration of the People's Republic of China, 2006) one day later. As it moved westward, it underwent RI and turned into a super typhoon at 1800 UTC 29 August. During the RI process, subjective intensity forecasts underestimated the explosive intensification of Hinnamnor, which led to the maximum 24-h intensity forecast error reaching –20 m s^{-1} from the China Meteorological Administration (CMA) and –60 kt from the Joint Typhoon Warning Center (JTWC). While moving southwestward, a tropical depression merged with Hinnamnor and expanded its size in terms of the azimuthally averaged radius of gale-force (17 m s^{-1}) winds (R17). Hinnamnor gradually slowed down from 1800 UTC 31 August and wandered over the sea to the east of Taiwan and the Bashi Channel for about 60 h. During this period, Hinnamnor underwent RW to become a severe typhoon. During the RW process, the error resulting from the astonishing overestimation in the 24-h intensity forecast from CMA was up to 23 m s^{-1} on 1 September. Hinnamnor entered the East China Sea and moved northward early in the morning on 4 September. It then re-intensified to a super typhoon by 0300 UTC 4 September, gradually turned to the northeast and passed through the East China Sea, and underwent extratropical transition. Hinnamnor made landfall in the southern part of the Korean peninsula and caused great damage to the Republic of Korea before entering the Japan Sea in the morning on 6 September and transforming into an extratropical cyclone that night. This short article provides a brief summary of super typhoon Hinnamnor's features and the major scientific research opportunities presented by different stages of its lifespan.

2. Data and methods

The track and intensity (maximum wind speed) data analyzed here were collected from the official typhoon bulletins issued by the National Meteorological Center of the China Meteorological Administration (NMC/CMA), the Regional Specialized Meteorological Center (RSMC), Tokyo, and the Joint Typhoon Warning Center (JTWC), which provide this information at intervals of 3 h or 6 h. Daily microwave optimally interpolated sea surface temperature (SST) satellite data, which are used to reveal the SST and SST cooling caused by the TC, were taken from the Optimum Interpolation Sea Surface Temperature (OISST) dataset, which has a spatial resolution of 0.25° × 0.25° (https://psl.noaa.gov/data/gridded/data.noaa.oisst.v2.highres.html; Reynolds et al., 2007). Sea surface height anomaly and geostrophic current data were obtained from the Copernicus Marine Environment Monitoring Service and have a spatial resolution of 0.25° × 0.25° and a temporal resolution of 6 h (https://resources.marine.copernicus.eu/product-detail/). Gust and sea level pressure (SLP) data at four observation stations close to the TC center were acquired from the National Weather Information Center of the CMA. FY-4A visible imagery was downloaded from the National Satellite Meteorological Center (http://fy4.nsmc.org.cn/portal/cn/theme/FY4A.html). The atmospheric data used to calculate the extratropical transition parameters were taken from the daily reanalysis ERA5 product (Hersbach et al., 2020).

To compare TC intensities from different operational official agencies, the conversion relations proposed by Bai et al. (2022) is adopted. The RI threshold is defined as the 95th percentile of 24-h intensification rates, corresponding to a strengthening of 30 kt (15.4 m s^{-1}) or greater within 24 h over the western North Pacific (Kaplan and DeMaria, 2003). The RW threshold is defined as the 95th percentile of all 24-h over-water weakening rates, corresponding to a decrease in maximum surface wind of 40 kt (20.6 m s^{-1}) or greater over a 24-h period (Ma et al., 2019). The process of extratropical transition (ET) is defined using the cyclone phase space (CPS) threshold to determine the ET onset and completion times. CPS parameters indicate the storm-motion-relative thickness symmetry and thermal wind (Hart, 2003; Evans and Hart, 2003; Hart et al., 2006; Wang et al., 2012), and a cyclone symmetry parameter of $B > 10$ and upper-level thermal wind of $-V_T^U < 0$ indicate ET onset, while $B > 10$ and $-V_T^U < 0$ together with lower-level thermal wind $-V_T^L < 0$ indicate ET completion (Song et al., 2011).

3. Results

3.1. *Formation and RI*

Hinnamnor was the eleventh western North Pacific TC in 2022, forming over the vast warm ocean (where SSTs were greater than 29°C; Fig. 1) at 0600 UTC 28 August. The tropical Pacific was experiencing a persistent La Niña event (Fang et al., 2023), which led to an abnormally warmer SST than the climatology (anomalies of about 1.0°C–1.5°C) around the TC genesis location. High SSTs are conducive to an increase in local buoyancy and thereby promote TC formation, development, and intensification (Montgomery and Smith, 2014; Jaimes et al., 2015). Hinnamnor formed at a latitude of 25.9°N and was one of six western North Pacific TCs that formed north of 25°N in 2022. The unusual more northward TC genesis locations might have been related to the strong equatorial cold tongue associated with the La Niña event over the equatorial Pacific.

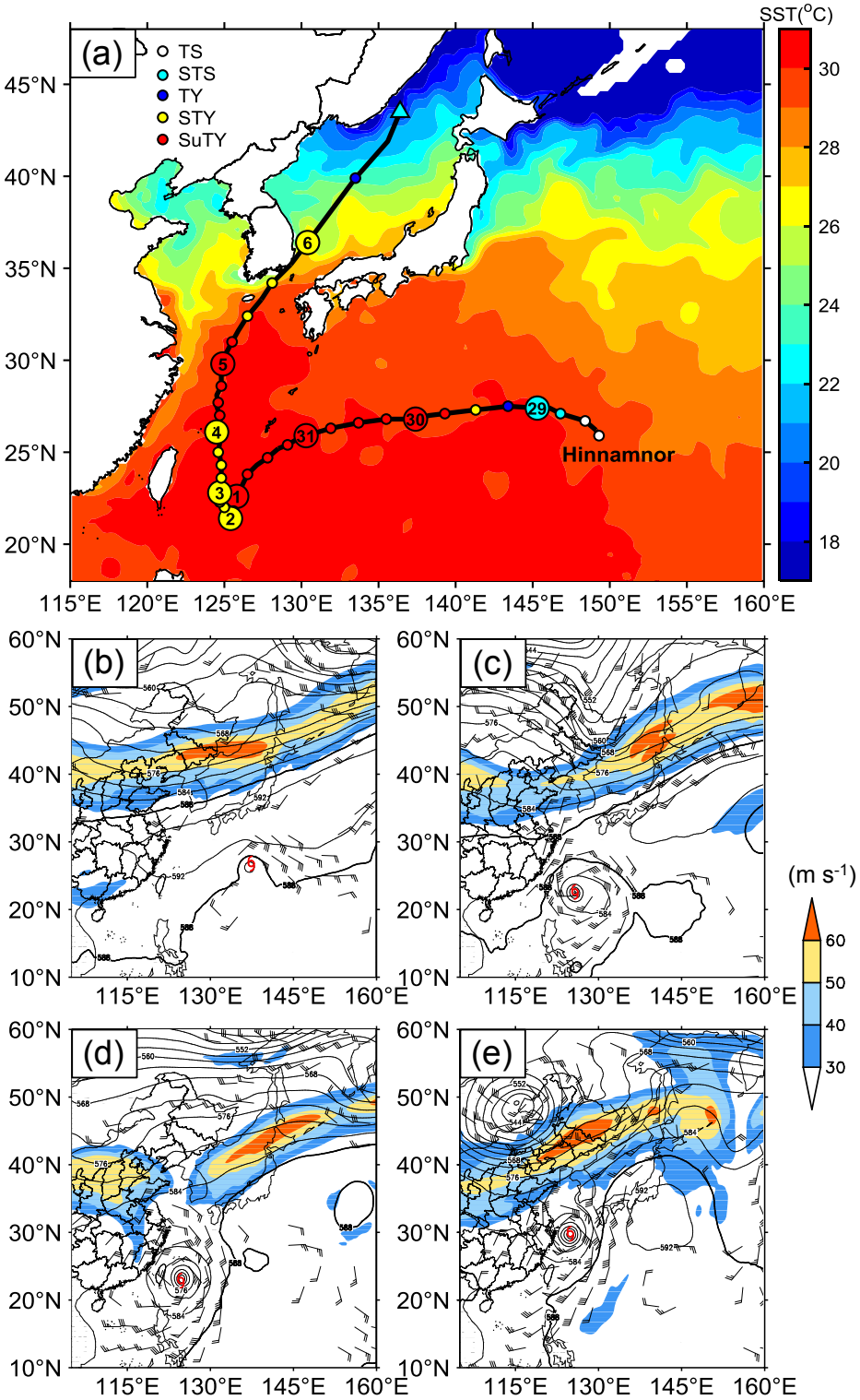

Fig. 1. (a) Hinnamnor's full track plotted over the SST on 28 August 2022 (shaded; units: °C). The TC intensity categories are based on the Criteria of Tropical Cyclones [GB/T 19201-2006 in General Administration of Quality Supervision, Inspection and Quarantine of the People's Republic of China (2006)] and include tropical storm (TS), severe tropical storm (STS), typhoon (TY), severe typhoon (STY), and super typhoon (SuTY). The triangle indicates an extratropical cyclone. The numbers inside the circles indicate the date. The 200-hPa jet (shaded while greater than 30 m s^{-1}, units: m s^{-1}), 500-hPa geopotential height (contours, bold at 588 dagpm, units: dagpm), and 850-hPa wind (barb while greater than 12 m s^{-1}, units: m s^{-1}) at 0000 UTC on (b) 30 August, (c) 1 September, (d) 3 September, and (e) 5 September.

Hinnamnor moved westward on the south side of the subtropical high, roughly following the steering air flow (Fig. 1b). As it moved westward, Hinnamnor intensified explosively from 23 m s^{-1} to 62 m s^{-1} (tropical storm to super typhoon) between 0900 UTC 28 August and 1200 UTC 30 August 2022 (Fig. 2a). The maximum intensification rate was 27 m s^{-1} within 24 h (identified by the operational data issued by the CMA). The continuous RI process lasted as long as 54 h; meanwhile, a secondary eyewall formation (SEF) occurred close to the time of Hinnamnor's maximum intensity. Hinnamnor completed the process of eyewall replacement in about 24 h and developed into a slightly smaller cyclone with an approximate 34-kt wind radius of 160 km (at 0000 UTC 31 August). During this eyewall replacement cycle, the issued bulletins from CMA, RSMC, and JTWC indicated a slight decrease in Hinnamnor's intensity.

3.2. *Vortex merger and size expansion*

As Hinnamnor approached the Ryukyu Islands, a tropical depression formed just 700 km to the south (Figs. 3a and b), and the subsequent vortex merger between it and Hinnamnor clearly involved the Fujiwara effect (Fujiwhara, 1921, 1923; Brand 1970). According to the revised model of this effect put forward by Lander and Holland (1993), binary TCs approach each other gradually within the first few hours, followed by a period of relatively stable cyclonic mutual-rotation, and then the last stage is a cyclonic merger or separation. In the present case, the two vortices began to rotate counterclockwise and gradually approached each other from 0600 UTC 30 August to 0000 UTC 1 September 2022; the visible satellite imagery shows an obvious vortex filamentation process happening to the tropical depression (Fig. 3c). Meanwhile, the translation speed of Hinnamnor was about 30 km h^{-1}, which is faster than the average speed of TCs at this latitude (Chen and Ding, 1979; Shanghai Typhoon Institute, China Meteorological Administration, 2017).

Subsequently, the diameter of Hinnamnor's cloud cover expanded from 320 km to approximately 520 km, as seen in the satellite visible imagery (Figs. 3b–d). Based on the TC bulletins issued by JTWC, Hinnamnor's analyzed R34, which is the azimuthally averaged radius of gale-force (34-kt or approximately 17.5-m s^{-1}) winds, increased in all four quadrants. In the northwest quadrant, R34 increased from 50 miles to 280 miles (approximately 80 km to 450 km); in the northeast, south-

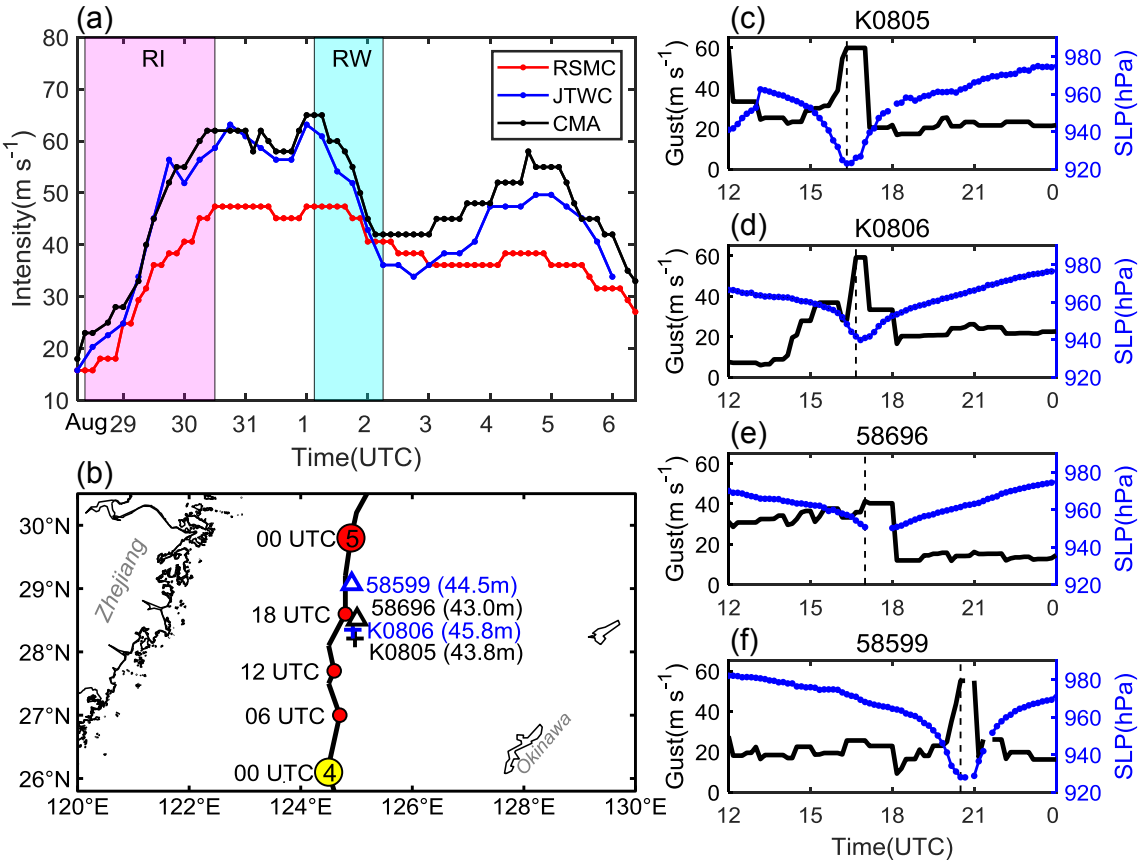

Fig. 2. (a) Hinnamnor (2022)'s intensity (maximum sustained wind speed; units: m s^{-1}), where the black, red, and blue lines represent the data from the CMA, RSMC Tokyo, and JTWC, respectively. (b) Hinnamnor's track (plot) in the southern part of the East China Sea and the station positions (crosses and triangles). The two crosses denote stations K0805 and K0806, and the two triangles denote the Chunxiao (58696) and Pinghu (58599) oil platforms. The height of each station is indicated in bracket. (c–f) Gusts (black lines; units: m s^{-1}) and SLP (blue lines; units: hPa) observed at stations (c) K0805, (d) K0806, (e) 58696, and (f) 58599 on 4 September.

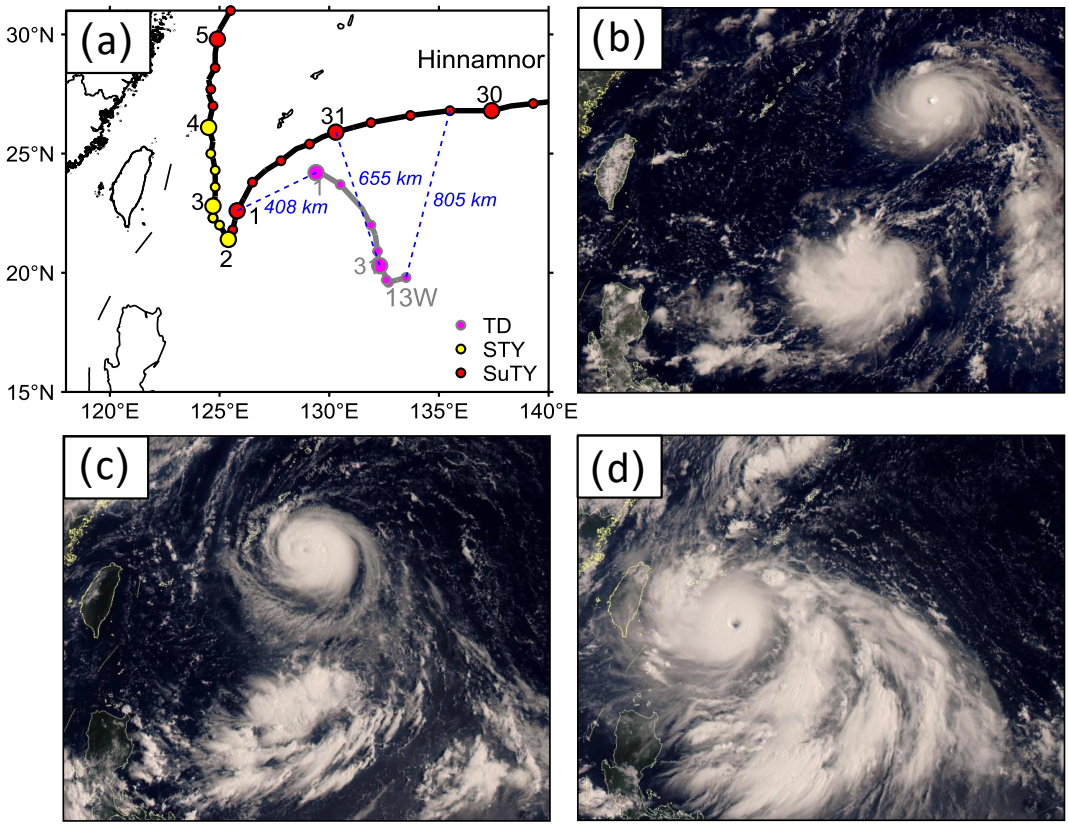

Fig. 3. (a) Tracks of Hinnamnor (2022) and the tropical depression (13W) with which it merged. The numbers beside the circles indicate the date. (b–d) FY-4A visible imagery (0.65 μm) at (b) 0600 UTC 31 August, (c) 0000 UTC 31 August, and (d) 0000 UTC 1 September 2022.

west, and southeast quadrants, R34 enlarged from 50 miles to 200 miles (approximately 80 km to 320 km) on average. Hinnamnor's size increased in terms of both R34 and R50 (azimuthally averaged radius of 50-kt winds), i. e., both the inner core and outer core expanded in the process of the merger, as previously described by Wang and Wang (2013).

During the merger, the dry air of the subtropical high between the two cyclones intruded into Hinnamnor. Dragging a huge spiral cloud band, the cyclone moved southwestward and began to slow down on 1 September (Fig. 3d). Settled inside the subtropical high, Hinnamnor (2022) wandered over the sea to the east of the Bashi Channel (Figs. 1c and d).

3.3. *Cold wake and RW*

Hinnamnor's long residence time caused marked SST cooling over the sea to the east of Taiwan, which in turn acted to weaken the typhoon. The Dvorak-T (DT) number based on the Dvorak technique (Velden et al., 2006) dropped from 7.0 to 5.0, Hinnamnor was downgraded to a severe typhoon, and the maximum sustained wind speed decreased from 65 m s^{-1} to 42 m s^{-1} (super typhoon to severe typhoon status) from 0600 UTC 1 September to 0300 UTC 2 September. The weakening rate of Hinnamnor was 23 m s^{-1} within 18 h, making it an RW event.

The long residence time of the typhoon in this particular area was conducive to upwelling and vertical mixing across the mixed layer base and resulted in obvious cooling (Fig. 4). There was a hysteresis in the SST cooling after the typhoon passed; maximum cooling generally occurs 1–3 days after a typhoon passes, with 1 day being the most common (Dare and McBride, 2011). Consistently, the cooling on 4 September reached a maximum of −5.5°C (at 22.1°N, 126.0°E).

Ocean feedback plays an important role in the RW process because it can suppress the development of TCs (Wada and Chan, 2008; Lin et al., 2013). Typhoons can cause upwelling in the ocean and divergence of surface seawater, which is consistent with the cyclonic structure of cold eddies in the ocean. Therefore, cold eddies will be generated or enhanced, and the effect of upwelling will be enhanced after a typhoon passes.

3.4. *Sudden change in track and re-intensification*

Meanwhile, the eastward movement of the midlatitude trough helped the eastward retreat of the subtropical high, which led to the break of the belt-like subtropical high and resulted in a northward steering flow; therefore, Hinnamnor turned northward (Figs. 1c and d). Abruptly recurving TC tracks are challenging to forecast (Rappaport et al., 2009), and poor forecasting of such abnormal cases has socioeconomic impacts (Galarneau and Davis, 2013). A TC with an abnormal

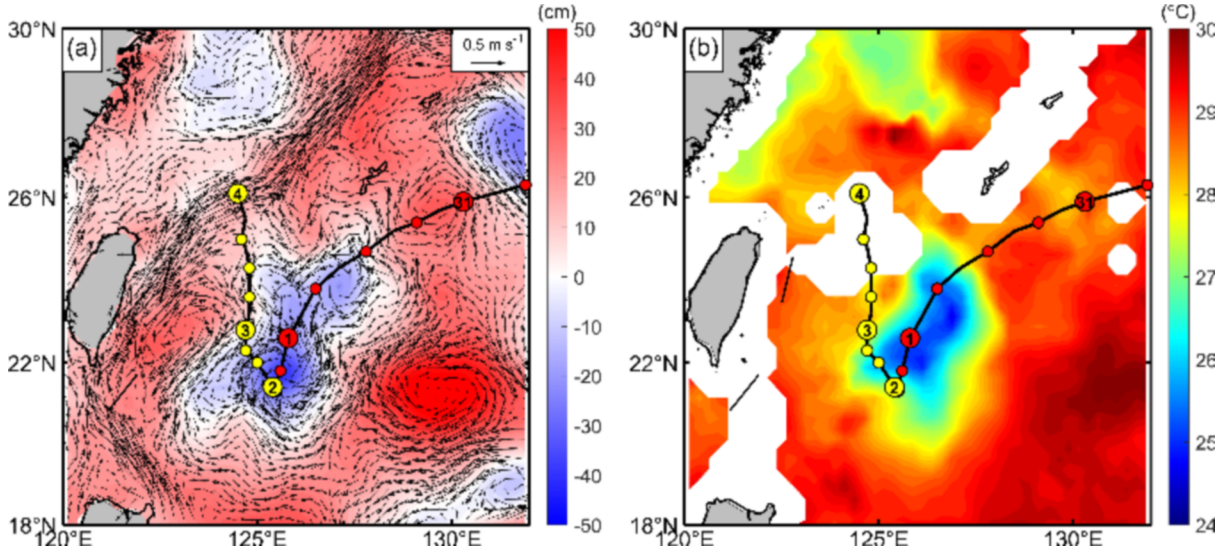

Fig. 4. (a) Sea surface height anomaly (shaded; units: cm) and currents (vectors), and (b) SST (shaded; units: °C) on 4 September 2022. Hinnamnor's track and intensity is the same as in Fig. 1.

track is always involved in complex interactions with its surrounding systems and thus has low predictability (Shi et al., 2014). The position of the curving point is difficult to forecast several days in advance (Chen et al., 2012). In the present case, during 0600 UTC 28 to 0000 UTC 29 August, the averaged 48- and 72-h track forecast errors were 221 km and 560 km, respectively. Both were significantly larger than the average from 2016 to 2020, which were 129 km and 196 km, respectively (Chen et al., 2022). Several days ahead of Hinnamnor recurving, the subjective track forecast errors were enormous. For example, the official track forecast released by CMA at 0000 UTC on 29 August led to the 72-, 96-, and 120-h track forecast errors reaching 636 km, 688 km, and 511 km, respectively, which illustrates the track forecast difficulties when the sudden track change happened.

During 3–5 September, Hinnamnor crossed the Kuroshio and moved into the East China Sea with an increased translational speed (approximately 20 km h^{-1}). The originally weakened eyewall had been strengthened again, and a secondary eyewall had formed. The re-intensified typhoon had a tiny eye; the diameter of the inner eyewall was only 30 km. The Hangzhou Bay area recorded a maximum 2-min average wind of 29.1 m s^{-1} and gusts of up to 35.7 m s^{-1}. The oil platform in the central East China Sea (station K0805) observed a maximum average wind of 35.0 m s^{-1} and a maximum gust of 60.0 m s^{-1}, along with a minimum SLP of 923.0 hPa captured at 1620 UTC 4 September (Fig. 2c), just as the northeast-quarter eyewall passed by. Station K0806 recorded a maximum average wind of 46.6 m s^{-1} and a maximum gust of 59.3 m s^{-1} just 20 min later (Fig. 2d). Pinghu oil platform (station 58599) recorded a maximum gust of 59.3 m s^{-1} and a minimum SLP of 927.9 hPa at 2030 UTC 4 September (Fig. 2f). These in situ observations clearly depict the passage of the typhoon eye. The concentric eyewall (CE) structure was maintained for a very long time.

3.5. *Extratropical transition*

In the northern part of the East China Sea, northward-moving Hinnamnor encountered an eastward-moving midlatitude low (Fig. 1e), accelerated to move northeastward, and underwent ET afterward (Fig. 5). The ET process determined by the CPS was from 1800 UTC 5 September to 0900 UTC 6 September (Fig. 5a; Song et al., 2011; Wang et al., 2012). Hinnamnor passed to the east sea of Jeju Island and made landfall in Geoje, South Gyeongsang Province, South Korea as a severe typhoon (45 m s^{-1}, 950 hPa) at around 1850 UTC 5 September. Interacting with the midlatitude low to its northwest (Fig. 5b), Hinnamnor then turned into a frontal cyclone in the evening on 6 September (Kitabatake, 2011). The CMA, RSMC-Tokyo, and JTWC all issued an extratropical cyclone warning over the northern part of the Japan Sea on 1200 UTC 6 September.

The cyclone during its ET process caused great damage to South Korea with its strong winds and heavy rainfall, becoming one of the typhoons with the greatest ever impact in South Korea's history.

4. Concluding remarks

Based on multiple sources of observational and reanalysis data, it was confirmed that Hinnamnor (2022) experienced RI, binary TC interaction and merging, size expansion, a sudden track change, RW, a strong cold wake, eyewall replacement cycles, and ET. These phenomena, and especially the scientific questions underpinning them, are all at the forefront of current

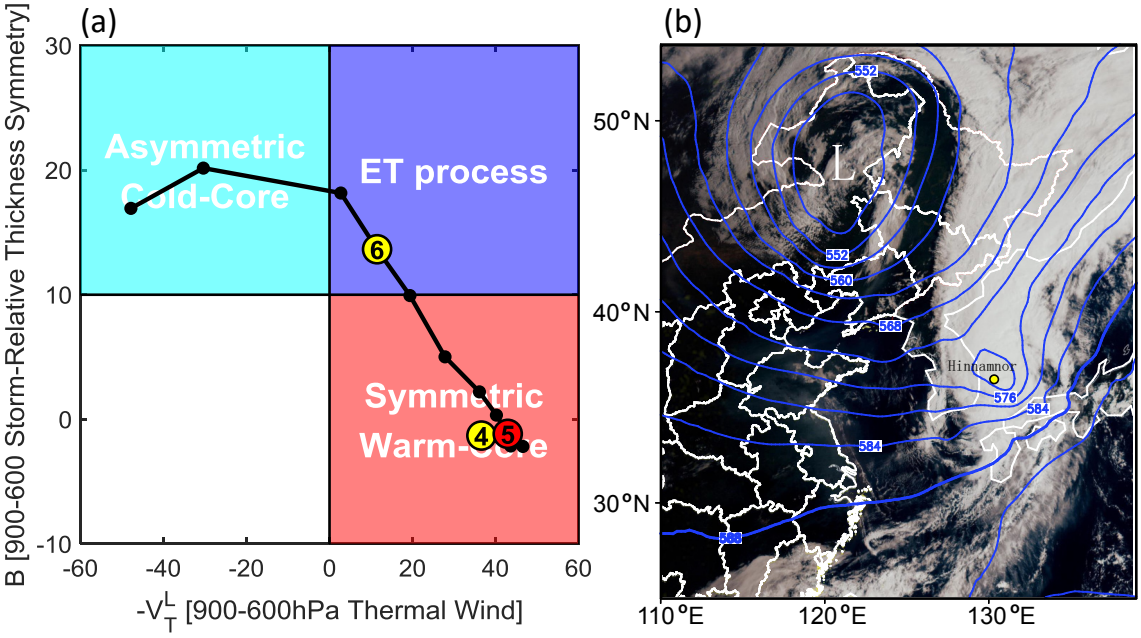

Fig. 5. (a) CPS parameters B (units: m) and $-V_T^L$ at 6-h intervals from 0000 UTC 4 to 1800 UTC 6 September 2022. The numbers inside the circles indicate the date. (b) FY-4A visible imagery (0.65 μm) and 500-hPa geopotential height (blue contours; units: dagpm) at 0000 UTC 6 September 2022. "L" denotes the midlatitude low, and the yellow dot represents the center of typhoon Hinnamnor (2022).

typhoon research (Wang and Wu, 2004; Emanuel, 2018; Lei, 2020). More interestingly, we can see that these phenomena were interconnected, such as the sudden track change and RW; the binary TC interaction, merger, and size expansion; and the eyewall replacement cycles and re-intensification. This motivates us to conduct synthesized analyses of TC track, intensity, and structural changes in future studies because of their obvious interplays. Indeed, this has recently been highlighted as a new paradigm in TC research by Tan et al. (2022). The remarkable lifespan of Super Typhoon Hinnamnor (2022), existing for 222 h and travelling 5574.38 km, should promote a wealth of future research.

Subjective forecast errors during periods of rapid TC intensity changes are astonishing, and these forecast errors greatly affect disaster risk reduction affairs and sometimes cause additional loss in maritime economic activities due to over-warning of TC intensity (Chen et al., 2012; Wang, 2018; DeMaria et al., 2021). Research on RI and RW, along with the ability to forecast and provide early warning for TC impacts under global warming, should be strengthened in the future (Wang et al., 2022; Wu et al., 2022). This paper suggests the importance of focusing more research on topics such as how air–sea interactions are reflected in the RW process and how the mesoscale and small-scale convection within the TC inner core affect the TC structure during the TC re-intensification process and ET process.

Acknowledgements. This work was supported in part by the National Science Foundation of China (Grant Nos. 42192554, 41876011, 61827901, and 41775065), the National Key Research and Development Program of China (Grant Nos. 2020YFE0201900 and 2022YFC3004200), Shanghai Typhoon Research Foundation (TFJJ202201), S&T Development Fund of CAMS 2022KJ012, and Basic Research Fund of CAMS 2022Y006.

REFERENCES

Bai, L. N., J. Tang, R. Guo, S. Zhang, and K. Y. Liu, 2022: Quantifying interagency differences in intensity estimations of Super Typhoon Lekima (2019). *Frontiers of Earth Science*, **16**, 5–16, https://doi.org/10.1007/s11707-020-0866-5.

Brand, S., 1970: Interaction of binary tropical cyclones of the Western North Pacific Ocean. *J. Appl. Meteorol.*, **9**(3), 433–441, https://doi.org/10.1175/1520-0450(1970)009<0433:IOBTCO>2.0.CO;2.

Chen, G. M., M. Q. Yang, X. P. Zhang, L. N. Bai, R. J. Wan, and Q. Cao, 2022: Verification on forecasts of typhoons over western North Pacific and South China Sea in 2020. *Meteorological Monthly*, **48**(4), 516–525, https://doi.org/10.7519/j.issn.1000-0526.2022.022101. (in Chinese with English abstract)

Chen, L. S., and Y. H. Ding, 1979: *An Introduction to the Western Pacific Typhoon*. Science Press, 491 pp. (in Chinese)

Chen, L. S., Y. Li, and Z. Q. Cheng, 2010: An overview of research and forecasting on rainfall associated with landfalling tropical cyclones. *Adv. Atmos. Sci.*, **27**, 967–976, https://doi.org/10.1007/s00376-010-8171-y.

Chen, L. S., Y. H. Duan, L. L. Song, and Y. L. Xu, 2012: *Typhoon Forecast and Disaster*. China Meteorological Press, 370 pp. (in Chinese)

Dare, R. A., and J. L. McBride, 2011: Sea surface temperature response to tropical cyclones. *Mon. Wea. Rev.*, **139**(12), 3798–3808, https://doi.org/10.1175/MWR-D-10-05019.1.

DeMaria, M., C. R. Sampson, J. A. Knaff, and K. D. Musgrave, 2014: Is tropical cyclone intensity guidance improving. *Bull. Amer. Meteor. Soc.*, **95**(3), 387–398, https://doi.org/10.1175/BAMS-D-12-00240.1.

DeMaria, M., J. L. Franklin, M. J. Onderlinde, and J. Kaplan, 2021: Operational forecasting of tropical cyclone rapid intensification at the national hurricane center. *Atmosphere*, **12**(6), 683, https://doi.org/10.3390/atmos12060683.

Duan, Y. H., L. S. Chen, J. Y. Liang, Y. Wang, L. G. Wu, X. P. Cui, L. M. Ma, and Q. Q. Li, 2014: Research progress in the unusual variations of typhoons before and after landfalling. *Acta Meteorologica Sinica*, **72**, 969–986, https://doi.org/10.11676/qxxb2014.085. (in Chinese with English abstract)

Duan, Y. H., and Coauthors, 2019: Landfalling tropical cyclone research project (LTCRP) in China. *Bull. Amer. Meteor. Soc.*, **100**(12), ES447–ES472, https://doi.org/10.1175/BAMS-D-18-0241.1.

Elsberry, L. E., L.-S. Chen, J. Davidson, R. Rogers, Y. Q. Wang, and L. G. Wu, 2013: Advances in understanding and forecasting rapidly changing phenomena in tropical cyclones. *Tropical Cyclone Research and Review*, **2**, 13–24, https://doi.org/10.6057/2013TCRR01.02.

Emanuel, K., 2018: 100 Years of progress in tropical cyclone research. *Meteor. Monogr.*, **59**(1), 15.1–15.68, https://doi.org/10.1175/AMSMONOGRAPHS-D-18-0016.1.

Evans, J. L., and R. E. Hart, 2003: Objective indicators of the onset and completion of ET for Atlantic tropical cyclones. *Mon. Wea. Rev.*, **131**, 909–925, https://doi.org/10.1175/1520-0493(2003)131<0909:OIOTLC>2.0.CO;2.

Fang, X. H., and Coauthors, 2023: Will the historic southeasterly wind over the equatorial Pacific in March 2022 trigger a third-year La Niña event. *Adv. Atmos. Sci.*, **40**(1), 6–13, https://doi.org/10.1007/s00376-022-2147-6.

Fei, R., J. Xu, Y. Q. Wang, and C. Yang, 2020: Factors affecting the weakening rate of tropical cyclones over the western North Pacific. *Mon. Wea. Rev.*, **148**(9), 3693–3712, https://doi.org/10.1175/MWR-D-19-0356.1.

Fujiwhara, S., 1921: The natural tendency towards symmetry of motion and its application as a principle in meteorology. *Quart. J. Roy. Meteor. Soc.*, **47**, 287–292, https://doi.org/10.1002/qj.49704720010.

Fujiwhara, S., 1923: On the growth and decay of vortical systems. *Quart. J. Roy. Meteor. Soc.*, **49**, 75–104, https://doi.org/10.1002/qj.49704920602.

Galarneau, T. J., and C. A. Davis, 2013: Diagnosing forecast errors in tropical cyclone motion. *Mon. Wea. Rev.*, **141**(2), 405–430, https://doi.org/10.1175/MWR-D-12-00071.1.

General Administration of Quality Supervision, Inspection and Quarantine of the People's Republic of China, Standardization Administration of the People's Republic of China, 2006: GB/T 19201-2006 Grade of Tropical Cyclones. Standards Press of China. (in Chinese)

Gray, W. M., 1968: Global view of the origin of tropical disturbances and storms. *Mon. Wea. Rev.*, **96**(10), 669–700, https://doi.org/10.1175/1520-0493(1968)096<0669:GVOTOO>2.0.CO;2.

Hart, R. E., 2003: A cyclone phase space derived from thermal wind and thermal asymmetry. *Mon. Wea. Rev.*, **131**, 585–616, https://doi.org/10.1175/1520-0493(2003)131<0585:ACPSDF>2.0.CO;2.

Hart, R. E., J. L. Evans, and C. Evans, 2006: Synoptic composites of the extratropical transition life cycle of North Atlantic tropical cyclones: Factors determining posttransition evolution. *Mon. Wea. Rev.*, **134**, 553–578, https://doi.org/10.1175/MWR3082.1.

Hersbach, H., and Coauthors, 2020: The ERA5 global reanalysis. *Quart. J. Roy. Meteor. Soc.*, **146**(730), 1999–2049, https://doi.org/10.1002/qj.3803.

Jaimes, B., L. K. Shay, and E. W.Uhlhorn, 2015: Enthalpy and momentum fluxes during Hurricane Earl relative to underlying ocean features. *Mon. Wea. Rev.*, **143**(1), 111–131, https://doi.org/10.1175/MWR-D-13-00277.1.

Kaplan, J., and M. DeMaria, 2003: Large-scale characteristics of rapidly intensifying tropical cyclones in the North Atlantic basin. *Wea. Forecasting*, **18**(6), 1093–1108, https://doi.org/10.1175/1520-0434(2003)018<1093:LCORIT>2.0.CO;2.

Kitabatake, N., 2011: Climatology of extratropical transition of tropical cyclones in the western North Pacific defined by using cyclone phase space. *J. Meteor. Soc. Japan*, **89**(4), 309–325, https://doi.org/10.2151/jmsj.2011-402.

Lander, M., and G. J. Holland, 1993: On the interaction of tropical-cyclone-scale vortices. I: Observations. *Quart. J. Roy. Meteor. Soc.*, **119**(514), 1347–1361, https://doi.org/10.1002/qj.49711951406.

Lei, X. T., 2020: Overview of the development history of China's typhoon research and operational work in the past century. *Science China Earth Sciences*, **63**, 362–383, https://doi.org/10.1007/s11430-018-9379-8.

Lin, I.-I., and Coauthors, 2013: An ocean coupling potential intensity index for tropical cyclones. *Geophys. Res. Lett.*, **40**(9), 1878–1882, https://doi.org/10.1002/grl.50091.

Ma, Z. H., J. F. Fei, and X. G. Huang, 2019: A definition of rapid weakening for tropical cyclones over the western North Pacific. *Geophys. Res. Lett.*, **46**(20), 11 471–11 478, https://doi.org/10.1029/2019GL085090.

Montgomery, M. T., and R. K. Smith, 2014: Paradigms for tropical-cyclone intensification. *Australian Meteorological and Oceanographic Journal*, **64**, 37–66, https://doi.org/10.22499/2.6401.005.

Rappaport, E. N., and Coauthors, 2009: Advances and challenges at the National Hurricane Center. *Wea. Forecasting*, **24**(2), 395–419, https://doi.org/10.1175/2008WAF2222128.1.

Reynolds, R. W., T. M. Smith, C. Y. Liu, D. B. Chelton, K. S. Casey, and M. G. Schlax, 2007: Daily high-resolution-blended analyses for sea surface temperature. *J. Climate*, **20**(22), 5473–5496, https://doi.org/10.1175/2007JCLI1824.1.

Rogers, R., and Coauthors, 2013: NOAA's hurricane intensity forecasting experiment: A progress report. *Bull. Amer. Meteor. Soc.*, **94**(6), 859–882, https://doi.org/10.1175/BAMS-D-12-00089.1.

Shanghai Typhoon Institute, China Meteorological Administration, 2017: *Climatological Atlas of Tropical Cyclones over the Western*

North Pacific (1981–2010). Science Press, 200 pp. (in Chinese)

Shi, W. L., J. F. Fei, X. G. Huang, X. P. Cheng, J. L. Ding, and Y. Q. He, 2014: A numerical study on the combined effect of Midlatitude and low-latitude systems on the abrupt track deflection of typhoon Megi (2010). *Mon. Wea. Rev.*, **142**(7), 2483–2501, https://doi.org/10.1175/MWR-D-13-00283.1.

Song, J. J., J. J. Han, and Y. Wang, 2011: Cyclone phase space characteristics of the extratropical transitioning tropical cyclones over the western North Pacific. *Acta Meteorologica Sinica*, **25**, 78–90, https://doi.org/10.1007/s13351-011-0006-y.

Tan, Z. M., L. L. Lei, Y. Q. Wang, Y. L. Xu, and Y. Zhang, 2022: Typhoon track, intensity, and structure: From theory to prediction. *Adv. Atmos. Sci.*, **39**, 1789–1799, https://doi.org/10.1007/s00376-022-2212-1.

Velden, C., and Coauthors, 2006: The Dvorak tropical cyclone intensity estimation technique: A satellite-based method that has endured for over 30 years. *Bull. Amer. Meteor. Soc.*, **87**(9), 1195–1210, https://doi.org/10.1175/BAMS-87-9-1195.

Wada, A., and J. C. L. Chan, 2008: Relationship between typhoon activity and upper ocean heat content. *Geophys. Res. Lett.*, **35**, L17603, https://doi.org/10.1029/2008GL035129.

Wang, Q., 2018: Forecast performance and study on RI process of typhoons Rammasun (1409) and Hato (1713). *TECO of Typhoon Committee 50th Session*, Ha Noi, ESCAP/WMO, 36 pp.

Wang, Q., Q. Q. Li, and G. Fu, 2012: Determining the extratropical transition onset and completion times of typhoons Mindulle (2004) and Yagi (2006) using four methods. *Wea. Forecasting*, **27**(6), 1394–1412, https://doi.org/10.1175/WAF-D-11-00148.1.

Wang, Y., and C. C. Wu, 2004: Current understanding of tropical cyclone structure and intensity changes-A review. *Meteorol. Atmos. Phys.*, **87**, 257–278, https://doi.org/10.1007/s00703-003-0055-6.

Wang, Y. Q., and H. Wang, 2013: The inner-core size increase of Typhoon Megi (2010) during its rapid intensification phase. *Tropical Cyclone Research and Review*, **2**, 65–80, https://doi.org/10.6057/2013TCRR02.01.

Wang, Y. Q., J. Xu, and Z. M. Tan, 2022: Contribution of dissipative heating to the intensity dependence of tropical cyclone intensification. *J. Atmos. Sci.*, **79**, 2169–2180, https://doi.org/10.1175/JAS-D-22-0012.1.

Wu, L. G., H. K. Zhao, C. Wang, J. Cao, and J. Liang, 2022: Understanding of the effect of climate change on tropical cyclone intensity: A review. *Adv. Atmos. Sci.*, **39**(2), 205–221, https://doi.org/10.1007/s00376-021-1026-x.

Zhao, D. J., H. X. Xu, Y. B. Yu, and L. S. Chen, 2022a: Identification of synoptic patterns for extreme rainfall events associated with landfalling typhoons in China during 1960–2020. *Advances in Climate Change Research*, **13**(5), 651–665, https://doi.org/10.1016/j.accre.2022.07.002.

Zhao, D. J., W. H. Gao, H. X. Xu, Y. B. Yu, and L. S. Chen, 2022b: A modeling study of cloud physical properties of extreme and non-extreme precipitation in landfalling typhoons over China. *Atmospheric Research*, **277**, 106311, https://doi.org/10.1016/j.atmosres.2022.106311.